Biochimica et Biophysica Acta 1848 (2015) 1656–1670

Contents lists available at ScienceDirect

Biochimica et Biophysica Acta

journal homepage: www.elsevier.com/locate/bbamem

C_8-glycosphingolipids preferentially insert into tumor cell membranes and promote chemotherapeutic drug uptake

Lília R. Cordeiro Pedrosa [a], Wiggert A. van Cappellen [b], Barbara Steurer [a], Dalila Ciceri [f,g], Timo L.M. ten Hagen [a], Alexander M.M. Eggermont [a,d], Marcel Verheij [c,e], Felix María Goñi [f,g], Gerben A. Koning [a,*], F.-Xabier Contreras [f,g,h,**]

[a] Laboratory Experimental Surgical Oncology, Section Surgical Oncology, Department of Surgery, Erasmus MC Cancer Center, Rotterdam 3000 CA, The Netherlands
[b] Optical Imaging Center, Department of Pathology, Erasmus MC, Rotterdam 3000 CA, The Netherlands
[c] Division of Biological Stress Response, The Netherlands Cancer Institute–Antoni van Leeuwenhoek Hospital, Amsterdam 1066 CX, The Netherlands
[d] Institut de Cancerologie Gustave Roussy, Villejuif, Paris 94800, France
[e] Department of Radiotherapy, The Netherlands Cancer Institute–Antoni van Leeuwenhoek Hospital, Amsterdam 1066 CX, The Netherlands
[f] Unidad de Biofísica (CSIC, UPV/EHU), P.O. Box 644, 48080 Bilbao, Spain
[g] Departamento de Bioquímica, Universidad del País Vasco, P.O. Box 644, 48080 Bilbao, Spain
[h] IKERBASQUE, Basque Foundation for Science, 48011 Bilbao, Spain

ARTICLE INFO

Article history:
Received 3 December 2014
Received in revised form 15 April 2015
Accepted 19 April 2015
Available online 24 April 2015

Keywords:
Short-chain glycosphingolipid
Tumor-cell membrane-permeability modulation
Targeting tumor cell membrane
Liposome
Doxorubicin

ABSTRACT

Insufficient drug delivery into tumor cells limits the therapeutic efficacy of chemotherapy. Co-delivery of liposome-encapsulated drug and synthetic short-chain glycosphingolipids (SC-GSLs) significantly improved drug bioavailability by enhancing intracellular drug uptake. Investigating the mechanisms underlying this SC-GSL-mediated drug uptake enhancement is the aim of this study. Fluorescence microscopy was used to visualize the cell membrane lipid transfer intracellular fate of fluorescently labeled C_6-NBD-GalCer incorporated in liposomes in tumor and non-tumor cells. Additionally click chemistry was applied to image and quantify native SC-GSLs in tumor and non-tumor cell membranes. SC-GSL-mediated flip-flop was investigated in model membranes to confirm membrane-incorporation of SC-GSL and its effect on membrane remodeling. SC-GSL enriched liposomes containing doxorubicin (Dox) were incubated at 4 °C and 37 °C and intracellular drug uptake was studied in comparison to standard liposomes and free Dox.

SC-GSL transfer to the cell membrane was independent of liposomal uptake and the majority of the transferred lipid remained in the plasma membrane. The transfer of SC-GSL was tumor cell-specific and induced membrane rearrangement as evidenced by a transbilayer flip-flop of pyrene-SM. However, pore formation was measured, as leakage of hydrophilic fluorescent probes was not observed. Moreover, drug uptake appeared to be mediated by SC-GSLs. SC-GSLs enhanced the interaction of doxorubicin (Dox) with the outer leaflet of the plasma membrane of tumor cells at 4 °C. Our results demonstrate that SC-GSLs preferentially insert into tumor cell plasma membranes enhancing cell intrinsic capacity to translocate amphiphilic drugs such as Dox across the membrane via a biophysical process.

1. Introduction

Ineffective outcome of chemotherapy is often due to dose-limiting toxic side effects of free drug and to reduced drug bioavailability in tumor cells. Liposomal drug carrier technology is extensively described as an effective means to prevent drug toxicity by minimizing drug interaction with healthy tissue [1–3]. Caelyx® or Doxil®, a formulation of doxorubicin (Dox) encapsulated in PEGylated, 85–100 nm liposomes (PLD) [4,5] is approved by EMA in Europe and by FDA in USA, for treatment of AIDS-related Kaposi's sarcoma [6], refractory ovarian cancer [7], myeloma [8] and metastatic breast cancer [6,9]. Although PLD accumulates in tumor due to its favorable pharmacokinetic profile and small particle size [10], its high stability prevents optimal drug accumulation

* Correspondence to: G A. Koning, Innovative Targeting Group, Laboratory Experimental Surgical Oncology, Section Surgical Oncology, Department of Surgery, Room Ee151b, Erasmus MC, 3000CA Rotterdam, PO Box 2040, The Netherlands. Tel.: +31 107043963; fax: +31 107044746.
** Correspondence to: F.-X. Contreras, Unidad de Biofísica, Centro Mixto Consejo Superior de Investigaciones Científicas–Universidad del País Vasco/Euskal Herriko Unibertsitatea (CSIC, UPV/EHU), Barrio Sarriena s/n, Leioa, Bizkaia 48940, Spain. Tel.: +34 94 601 2106; fax: +34 94 601 3360.
E-mail addresses: g.koning@erasmusmc.nl (G.A. Koning), xabier.contreras@ehu.es (F.-X. Contreras).

http://dx.doi.org/10.1016/j.bbamem.2015.04.011
0005-2736/

in tumor cells [11,12]. PLD's low drug bioavailability remains a main issue limiting its therapeutic efficacy [2,13]. A novel approach to enhance intracellular drug delivery in tumor cells was developed and involves insertion of short-chain glycosphingolipids (SC-GSLs), like C_8-glucosylceramide (C_8-GlcCer) or C_8-galactosylceramide (C_8-GalCer) in the tumor cell membrane, increasing its permeability to various anti-cancer drugs [14]. Co-delivery of SC-GSLs and drugs to tumor cells using liposomes as a nanocarrier caused higher levels of intracellular drug delivery specifically in tumor cells [15–18]. The mechanism underlying this SC-GSL mediated drug uptake enhancement and its preference for tumor cells is the subject of this study.

Sphingolipids contain a sphingosine backbone where the functional amino group at position C2 is acylated with a fatty acid (Fig. 1). One of the most investigated sphingolipids, ceramide has a free functional hydroxy group (−OH) at position C1, whereas in more complex sphingolipids this position is linked to a polar head group. In the particular case of GSLs, the head group corresponds to a sugar residue (i.e. glucose or galactose, among others). It has been described that long-chain ceramides, but not short-chain, have membrane remodeling properties when externally added or in situ generated in model membranes [19,20]. For instances, ceramides induce transbilayer lipid motion and increase membrane permeability in LUVs. Generation of non-lamellar structures by ceramide creates transitory lipid-packaging defects between lamellar and non-lamellar phases that account for the lipid scrambling and membrane permeability effects observed. In addition, it has been reported that both short (C2) and long-chain (C16) ceramides spontaneously form large stable pores in the outer mitochondrial membrane contributing to cytochrome c release during initiation of apoptosis [21]. Spontaneous formation of ceramide channels occurs by lateral segregation of ceramide chains parallel to the plane of the membrane with channel diameters of 0.8 nm for short-chain and up to 11 nm for long-chain ceramides [21]. Further, Samanta et al. were able to visualize C16-ceramide channels in a phospholipid membrane by transmission electron microscopy [22]. These channels consisted of columns of four to six ceramides H-bonded via amide groups and arranged as staves in either a parallel or anti-parallel manner. Differences in the biophysical interactions between ceramides and phospholipids are described to be dependent on the N-acyl chain length and the intra- and intermolecular hydrogen bonds between sphingolipids and surrounding lipids and lead to the formation of specific membrane domains, lipid sorting and create signaling platforms [20,23]. Yet, for SC-GSLs such as C_8-GlcCer or C8-GalCer little is known about possible mechanisms for domain formation and their role in enhancing drug transport. It is also known that C_6-ceramide does not enhance intracellular Dox uptake [14,17] which points to the effect of the GSL hydrophilic head group, such as C_8-GlcCer or C_8-GalCer, in the properties of short-chain GSLs as drug uptake enhancers.

In the present study, we aim at investigating the molecular mechanisms underlying SC-GSL- mediated cellular drug uptake and to study the cell type specificity of such mechanisms. To this end, the cellular fate of liposomes and SC-GSLs is investigated by confocal microscopy using fluorescently labeled SC-GSL (C_6-NBD-GalCer) and a stable liposomal bilayer marker DiD, a lipophilic tracer with markedly red-shifted fluorescence excitation and emission spectra. Studies are performed in tumor cells and normal cells to determine a possible preference for SC-GSL transfer to tumor cells. In addition, post-treatment click chemistry is applied in order to disturb as little as possible the original molecular structure of the lipid (C_8-GlcCer or C_8-GalCer) and its incorporation into cell membranes is imaged by microscopy and quantified by TLC. Finally new insights on SC-GSL mechanism of action as Dox uptake enhancers to tumor cells are studied at 4 °C and biophysical features of SC-GSLs are investigated using model membrane systems, due to the technical difficulties of investigating these molecular issues in vivo.

2. Materials and methods

2.1. Materials

Hydrogenated soy phosphatidylcholine (HSPC) and distearylphosphatidylethanolamine (DSPE)-PEG_{2000} were from Lipoid (Ludwigshaven, Germany). Short-chain glycosphingolipids, C_8 glucosyl(β) ceramide (d18:1/8:0) D-glucosyl-β-1,1′ N-octanoyl-D-erythro-sphingosine (C_8-GlcCer), C_8 galactosyl(β) ceramide (d18:1/8:0) D-galactosyl-β-1,1′ N-octanoyl-D-erythro-sphingosine (C_8-GalCer), C_6-NBD galactosyl ceramide N-[6-[(7-nitro-2-1,3-benzoxadiazol-4-yl)amino]hexanoyl]-D-galactosyl-β1-1′-sphingosine, egg-phosphatidylcholine (PC), phosphatidylethanolamine (PE), egg-sphingomyelin, liver phosphatidylinositol and brain PS were purchased from Avanti Polar Lipids (Alabaster, AL, USA) and the lipophilic tracer DiD ($C_{67}H_{103}ClN_2O_3S$) from Invitrogen, Carlsbad, USA.

Polycarbonate filters were from Northern Lipids (Vancouver, BC, Canada) and PD-10 Sephadex columns were from GE Healthcare (Diegem, Belgium). Cholesterol, Hepes (2-[4-(2-hydroxyethyl)-piperazin-1-yl] ethanesulfonic acid). Hoechst was from Molecular Probes (Leiden, The Netherlands). PBS was from Boom and FACS flow fluid from BD Biosciences. Dox-HCl (Dox) was from Pharmachemie (Haarlem, The Netherlands). Cholesterol (Chol) and Hepes (2-[4-(2-hydroxyethyl)piperazin-1-yl] ethanesulfonic acid) were from Sigma Aldrich (Zwijndrecht, The Netherlands). Pyrenebutyroyl-sphingomyelin (pyr-SM) was synthesized as described in Contreras et al. [24].

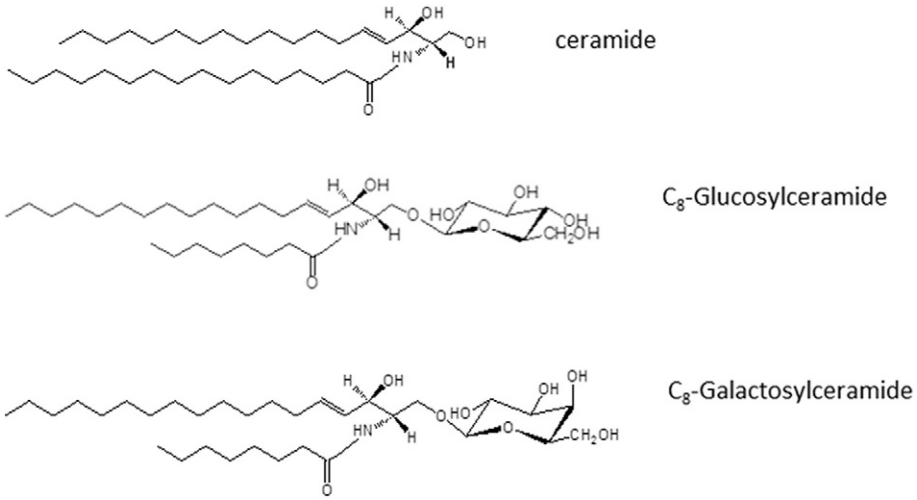

Fig. 1. Molecular structures of ceramide and short-chain glycosphingolipids (C_8-glucosyl and C_8-galactosyl). Molecular structures were design by Chem Draw Ultra 8.02.

2.2. Standard and SC-GSL-enriched liposomal formulations

Standard and SC-GSL-enriched liposomes were formulated of HSPC/cholesterol/ DSPE-PEG_{2000} in a molar ratio of 1.85:1:0.15. To the mixture of lipids, 0.1 mol of SC-GSL was added per mole of the total amount of lipid (including cholesterol).

Liposomes of 85–100 nm in diameter were prepared by lipid film hydration and extrusion method using a thermobarrel extruder, Northern Lipids, Vancouver, Canada at 65 °C [24].

Lipids were dissolved in chloroform-methanol 9:1 (v/v) mixed and a lipid film was created under a reduced pressure on a rotary evaporator and subsequently dried under a stream of nitrogen. Finally, lipid film was hydrated by 135 mM NaCl, 10 mM Hepes buffer, pH 7.4 and liposomes were sized by sequential extrusion through 100, 80, and 50 nm polycarbonate filters (Northern Lipids, Vancouver, Canada).

Fluorescent labeled liposomes and fluorescently labeled SC-GSL liposomes were prepared using the lipophilic tracer DiD, with markedly red-shifted fluorescence excitation and emission spectra (Invitrogen, Carlsbad, USA) and C_6-NBD galactosyl ceramide at 0.25 mol% of total amount of lipids. For fluorescently labeled SC-GSL liposomes, 0.25 mol% of C_6-NBD-GalCer is added to the SC-GSL liposomes, already containing 0.1 mol% of the respective SC-GSLs.

Hydration of the lipid film with $(NH_4)_2SO_4$ allowed loading of liposomes with Dox by a transmembrane ammonium sulfate gradient. Liposomes were loaded with Dox in a drug to phospholipid ratio of 0.1:1 (w/w) for 1 h at 65 °C [31]. Non-encapsulated Dox was removed by ultracentrifugation at 29,000 rpm for 1 h at 4 °C in a Beckman ultracentrifuge (Ti50.2 rotor). The liposome pellet was resuspended in a Hepes buffer (135 mM NaCl, 10 mM Hepes, pH 7.4). Size and polydispersity index (pdi) were determined at 25 °C by light scattering using a Zetasizer Nano ZS (Malvern Instruments, Malvern, UK). Lipid concentration was measured by phosphate assay [25].

2.3. Large unilamellar liposome's (LUV's) formulation

Large unilamellar liposome's (LUV's) mimicking plasma membrane lipid composition was composed of 17.5% (mol) PC, 5% (mol) PS, 5% (mol) PI, 10% (mol) PE, 50% (mol) Chol and 12.5% (mol) Egg- SM and formulated as described elsewhere [26]. Lipids that were dissolved in chloroform:methanol 2:1 (v/v) at the desired molar ratio and lipidic mixture were dried under a stream of nitrogen. To eliminate remaining traces of organic solvent, lipid mixture was placed in an exicator for 30 min under a vacuum. Resuspension of lipids was performed in a Hepes buffer (5 M KOH, 100 mM Hepes, pH 7.4), and then they were vigorously shaken with a vortex mixer to form multilamellar vesicles. The liposome suspension was frozen and thawed for 10 cycles. A single freeze–thaw cycle consisted of freezing for 2 min at liquid nitrogen temperature (−196 °C) and thawing for 5 min in a water bath at 50 °C. Liposomes were extruded by 10 passages through two filters of 100 nm (Nucleopore, Pleasanton CA) at room temperature. LUVs were kept on ice and used immediately after preparation.

2.4. Cell culture

All tumor cell lines (BLM melanoma, MDAMB-231 and SKBR-3 breast carcinoma, HeLa cervix carcinoma) were cultured in Dulbecco's modified Eagle medium, supplemented with 10% fetal calf serum and 4 mM L-glutamine. HUVEC was isolated by collagenase digestion and cultured in a HUVEC medium containing human endothelial serum-free medium (Invitrogen), 20% heat-inactivated newborn calf serum (Cambrex), 10% heat-inactivated human serum (Cambrex), 20 ng/ml human recombinant epidermal basic fibroblast growth factor (Peprotech EC Ltd) and 100 ng/ml human recombinant epidermal growth factor (Peprotech EC Ltd.) in fibronectin (Roche Diagnostics) coated flasks. Fibroblasts (3T3) were cultured in a Dulbecco's modified Eagle medium containing nutrient mixture F12, supplemented with 10% fetal calf serum and 4 mM L-glutamine. All serum supplements were heat-inactivated at 56 °C for 30 min. Cells were subcultured twice a week by trypsinization when a cell confluence of 80–90% was reached, and maintained in a water saturated atmosphere of 5% CO_2 at 37 °C. Tumor cells were seeded on a coating of 0.1% collagen (Invitrogen, Carlsbad, USA) in a culture medium and HUVEC was seeded on a coating of 1 mg/ml fibronectin in PBS (Roche, Rotkreuz, Switzerland) for microscopic imaging.

2.5. Liposomal, SC-GSL and drug fate studied by confocal microscopy

Laser scanning confocal microscopy (Zeiss LSM 510 META) was used to study the in vitro fate of fluorescently labeled liposomes with DiD or fluorescently labeled SC-GSL (C_6-NBD-GalCer) in SKBR3 cell after 2 h at 37 °C. C_6-NBD-GalCer was excited with the 488 nm line from an Argon ion laser, and emissions were detected between 505 nm and 550 nm. Dox was excited with a 543 nm helium–neon laser. Dox emissions were detected between 560 and 615 nm. The lipophilic tracer for liposomes, DiD was excited with a 633 nm helium–neon laser and near infrared emission was detected with a longpass 650 nm filter. Plasma membrane was stained by WGA 488 (wheat germ agglutinin from Invitrogen, Massachusetts, USA) to study co-localization of liposomes. The LysoTracker® Red DND-99 (Invitrogen, Carlsbad, USA) was incubated with cells in a concentration of 50 nM for 1 h at 37 °C. The dye was excited with 543 nm and emission was detected with a bandpass filter from 585 to 615 nm. Cells were imaged with a 63× planachromat oil (n.a. 1.4) objective lens.

For confocal experiments, $1 * 10^5$ cells were seeded on glass cover slides one day prior to imaging. Fluorescence intensity was quantified by ImageJ by separating two classes of fluorescence intensity (green as low and red as higher intensity) applying a high threshold to image the highest class intensity and membrane signal was selected and a Gaussian blur distribution after which the signal is split into 3 classes, background, low and high signals. Cells were imaged with a 63× plan-apochromat oil (n.a. 1.4) objective lens.

To address the question of possible SC-GSL internalization, live cell microscopy was performed in ascending focal planes in BLM, melanoma cells. Cells were incubated with C_6-NBD-GalCer liposomes and fluorescence was detected using a Zeiss ELYRA PS1 microscope equipped with a LSM 780 scanhead with high sensitivity GAsP detectors and excited with the 488 nm line from an argon ion laser, with emissions between 505 nm and 550 nm.

For time-lapse experiments, 10 positions on a slide were selected, and images were taken every 15 min in 4 focal planes for up to 14 h. The 633 nm He–Ne laser line was used for autofocus adjustments. In addition, quantification of cell-associated fluorescent lipid analogue using ImageJ software, yielded a 3 fold higher amount of fluorescence from C_6-NBD-GalCer enriched liposomes measured in the cell membrane of BLM, melanoma cells versus HUVEC, endothelial and 3T3, fibroblasts. The mean fluorescence intensity of a number of cells in each field of view was considered and subtracted from the background fluorescence, which was the same in all images of all cell lines studied. A mask was made as a thresholded area of a Gaussian blur image and was applied to select the cell membrane of the cells. Mean fluorescence intensities are compared to tumor and non-tumor cell membranes in time.

For confocal microscopy experiments at 4 °C, precooled cells were treated with a 40 μM Dox in a form of free drug, standard liposomes or 10% (mol) C_8-GalCer enriched liposomes diluted in a cold culture medium and incubated for 2 h at 4 °C. Cells were imaged before and after washing with a cold culture medium. Cells were kept on ice during experimental handling. Subsequently cells were further incubated for 2 h at 37 °C and 5% CO_2 and were imaged again before and after washing with a culture medium.

2.6. C_8-GlcCer cellular distribution and quantification by click chemistry

A clickable C_8-GlcCer or C_8-GalCer named as cC_8-GlcCer and cC_8-GalCer, respectively, containing a ω-terminal alkyne in the fatty acid was synthesized as described by Thiele et al. [25]. Addition of the ω-terminal alkyne maintains the original chemical properties of C_8-GlcCer or C_8-GalCer and allows the lipid detection by click chemistry with an azide-labeled fluorophore to localize and quantify the respective SC-GSLs transferred to the cell. The alkyne group is accessible to the azide once the lipid is inserted in the cell. Non-inserted lipid is washed off before fixation and labeling. To determine optimal lipid analogue concentration and incubation time, 10^5 HeLa cells were seeded in a 3.5 cm glass bottom dishes. After the treatment with 40 μM of C_8-GlcCer in ethanol/de-lipidated medium, cells were incubated for 1 h or 2 h. In parallel, cells were treated with 10 μM, 20 μM and 40 μM for 2 h at 37 °C, and 5% CO_2.

To determine SC-GSL transfer preferentially to tumor cells, BLM melanoma and MDAMB, breast carcinoma cells were treated with 10 μM cC_8-GlcCer or 10 μM cC_8-GalCer in free form and 100 μM cC_8-GlcCer co-inserted in liposomes. Non-tumor cells 3T3, fibroblasts were treated with the same lipid concentrations as tumor cells. Cells were washed twice in PBS and fixed at RT for 10 min with 4% PFA, sucrose and 4 mM EDTA in PBS 4%. After fixation, click chemistry was performed for 1 h at RT by adding a mixture of 0.1 M ascorbic acid, 1 mM $CuSO_4$ and 5 μM Cy3-azide in 1 mM Tris–HCl pH 8. Control cells were treated in the absence of $CuSO_4$ that catalyze the click chemistry reaction. To localize the lipid in the cell by fluorescence microscopy, additional nuclear and plasma membrane staining were performed with Hoescht (Molecular Probes, Leiden, The Netherlands) and WGA 488 (wheat germ agglutinin from Invitrogen, Massachusetts, USA), respectively. For SC-GSL quantification, cells were scraped and collected in 300 μl of PBS and centrifuged at 6500 rpm for 5 min at RT. Lipid extraction from equal amounts of cells and quantification were performed as described in Thiele et al. [25]. Fluorescence images were acquired with a digital UV Chromato-Vue cabinet (UVP, LLC).

2.7. Transbilayer redistribution of pyrene-SM by SC-GSL

The extent of a transbilayer lipid motion or flip-flop was measured in LUVs composed of 17,5 mol% PC; 5 mol% PS; 5 mol% PI; 10 mol% PE; 50 mol% Chol; and 12.5 mol% SM [26], by a method described by Müller et al. [27]. This method consists of an asymmetric incorporation of a pyrene fluorescent SM analogue (pyr-SM) inserted into the outer leaflet of the membrane and a further dilution of the probe within the inner and outer leaflets of the membrane upon a transbilayer redistribution induced by SC-GSL membrane interaction. pyr-SM can be present in the form of excimers (I_E) when in high concentrations in the outer leaflet or monomers (I_M) upon dilution of the probe to the inner leaflet of the cytoplasmic membrane displaying different emissions at 465 nm or 395 nm, respectively. Redistribution of pyr-SM from the outer to the inner leaflet can be followed by a decrease of the excimer and an increase in the monomer fluorescence, decreasing the ratio I_E/I_M. The transbilayer movement of pyr-SM in pure phospholipid vesicles is described as very slow causing a constant I_E/I_M. Experiments were performed at 37 °C in a spectrofluorometer AMINCO Bowman Series2. Lipid concentration was 300 μM for LUVs to which 15 μM of pyr-SM was added and incubated for 10 min at 37 °C prior to an addition of 15 μM of SC-GSL (C_8-GlcCer or C_8-GalCer and cC_8-GlcCer or cC_8-GalCer). Immediately after pyr-SM incorporation in the outer leaflet of the membrane, before any redistribution, I_E/I_M was set to 1. SC-GSL-induced flip-flop is represented by I_E/I_M ratio of pyr-SM upon incorporation of SC-GSL into the outer leaflet of the membrane. Control experiments were performed by adding ethanol, which was used as vehicle to deliver SC-GSL.

2.8. Leakage assay

Leakage of vesicular 8-aminonaphtalene-1,3,6-trisulfonate (ANTS)/p-xylene bispyridinium bromide (DPX) was assayed, as explained by Ellens et al. [28]. ANTS and DPX are water soluble anion/cation fluorophore quencher pair. ANTS fluorescence in the liposome (plasma membrane like LUVs) is quenched by collisional energy transfer to DPX. When both ANTS and DPX are trapped in the lumen of a vesicle, they exist in the form of a non-fluorescent complex. When vesicle efflux occurs, ANTS and DPX become diluted, the complex dissociates and free ANTS emits fluorescence. ANTS fluorescence spectrum has an excitation maximum at 350 nm and an emission maximum at 530 nm. A cut of filter of 450 nm was placed between the sample and the emission monochromator to avoid scattering interferences. Liposomes were prepared as described in Section 2.2. Non-encapsulated ANTS–DPX complex is removed by passing the liposomes through a Sephadex G-75 column. LUVS were prepared freshly for each experiment. A spectrofluorimeter Aminco Bowman Series 2 with a fluorescence set at 355 nm for excitation and 520 nm for emission in the presence of a filter of 450 nm to eliminate possible noise from the presence of liposomes, was used to measure differences in the fluorescence of ANTS–DPX complex under constant mixing at 37 °C. The basal signal of fluorescence was set to 0% before adding 15 μM of C_8-GlcCer or C_8-GalCer to 0.3 mM of the LUV's suspension. The fluorescence for 100% release was set after solubilizing liposomal membrane by adding Triton X-100 (10 mM final concentration in the cuvette).

2.9. Intracellular drug uptake by flow cytometry

Intracellular Dox levels in tumor BLM melanoma and non-tumor 3T3 fibroblasts were measured by flow cytometry. Cells were seeded on a flat bottom 24 well plate at a final concentration of 6×10^4 cells/well. After 24 h at 37 °C, 5% CO_2, cells were treated with 10 μM Dox in the form of standard liposomes containing doxorubicin (Dox), C_8-GlcCer or C_8-GalCer enriched liposomes diluted in the respective culture medium. After 24 h treatment, cells were washed twice with PBS to remove free drug and liposomes and cells were harvested by trypsinization. Cell suspensions were resuspended in a FACS buffer (168 mg EDTA, 2,5 mg BSA, 5 ml 10% NaN3 in PBS). Cell suspension was centrifuged at 400 rcf at 4 °C for 5 min. Cell pellets were resuspended in a 200 μl FACS buffer containing the FarRed (L10120) LIVE/DEAD® dead cell stain (Invitrogen, Carlsbad, USA) in a 1:1000 dilution. After 30 min at RT, cells were analyzed by flow cytometry (FACSCalibur, BD Biosciences). Healthy cells were selected by size (forward scatter), shape (sideward scatter) and viability (LIVE/DEAD stain, detected in FL4 channel, P653–669 nm). Cellular Dox uptake was measured by the fluorescent signal detected in the FL2 channel (BP 564–606 nm) after excitation with a 488 nm laser. Cell count was set to 10,000 cells. CellQuest™ software was used to analyze data.

2.10. Statistics

Data were analyzed using GraphPad Prism 5 software. Results of two-tailed, unpaired *t*-test are indicated by: not significant (ns) ($p > 0.05$), * ($p < 0.05$), ** ($p < 0.01$), and *** ($p < 0.001$).

3. Results

3.1. Liposome characterization

Dox-loaded or empty liposomes with and without SC-GSLs were prepared and characterized. Liposomes were obtained with sizes between 85 and 95 nm, a polydispersity index (pdi) of <0.1 and Dox-loading efficiency of >80%. Values for liposome size and pdi before (empty-L) and after loading with Dox, drug concentration, loading

efficiency and phospholipid (PL) recovery after ultracentrifugation (UC) are represented in Table 1.

3.2. SC-GSL transfer to cell membrane

SC-GSLs are described to enhance intracellular drug uptake from liposomes into tumor cells [15,17,18,29]. To investigate the behavior of SC-GSLs incorporated in liposomal bilayer when it contacts tumor cell membranes, live cell imaging was performed in SKBR3 cells. After 2 h incubation at 37 °C with fluorescently C_6-NBD-GalCer labeled liposomes (Fig. 2A), SC-GSLs were inserted throughout the tumor cell plasma membrane. Within the plasma membrane, SC-GSLs tended to accumulate in distinct areas with filopodia or lamellopodia like cellular protrusions (Fig. 2B). Those membrane modifications were observed once liposomes get in close contact with the plasma membrane (Supplemental Fig. 1), which supports SC-GSL transfer from liposomes to the plasma membrane [29].

Intracellular SC-GSL uptake was minor in comparison to the high levels of lipid in the cell membrane. In the cytoplasm, SC-GSL fluorescence intensities varied between 0 and 2000 AU. In contrast, lipid fluorescence reached a maximum intensity of 15,000 AU in the cell membrane (Fig. 2B). An illustration of the transfer of fluorescently labeled C_6-NBD-GalCer from liposomes in suspension (green) to the cell membrane is presented in Movie 1. The massive accumulation of the lipid in the cell membrane (red) is observed to occur in irregular structures that surrounded the cell surface in contrast to a low lipid concentration associated with liposomes in medium (green).

3.3. SC-GSL insertion into cell membrane is reversible

Next, we investigated a putative reversible mechanism of SC-GSL insertion into cellular membranes. To this end, ascending focal planes with a slide interval of 0.4 μm of BLM cells treated with fluorescently C_6-NBD-GalCer labeled liposomes for 2 h at 37 °C was performed (Fig. 3, middle panel). A massive lipid accumulation in the cell membrane with a higher incidence in specific areas was observed. Control BLM cells without SC-GSL treatment (left panel) showed some intracellular autofluorescent signal. Intensive washing of SC-GSL-liposome-treated cells with cold-PBS could remove a major part of the SC-GSL from the membrane (right panel) pointing to a reversible membrane interaction in the outer monolayer of the cell membrane. After washing, some SC-GSL fluorescence remained associated with cells.

3.4. Cellular fate of SC-GSLs and liposome

To unravel the mechanism of action of SC-GSLs as cellular drug uptake enhancers [17,18,29], we monitored the intracellular fate of fluorescently labeled liposomes in SKBR3 cells in relation to the SC-GSL fluorescent (Fig. 4). Dual labeled liposomes were used containing the blue lipophilic tracer DiD as a stable marker for the liposomal phospholipid bilayer and the green fluorescent lipid analogue C_6-NBD-GalCer as SC-GSL marker. After 2 h incubation at 37 °C, liposomal nanoparticles (DiD, blue) remained solely outside the cell, whereas SC-GSL (C_6-NBD-GalCer, green) accumulated in the plasma membrane and to a minor extent intracellularly. In parallel, intracellular colocalization of SC-GSL with lysosomes was performed. We observed a minor colocalization of C_6-NBD-GalCer (green) and lysotracker red, labeling acidic organelles (Fig. 4).

3.5. SC-GSL transfer is tumor cell specific

The plasma membrane undergoes continuous rearrangements through endo- and exocytosis. We studied the fate of C_6-NBD-GalCer in tumor and non-tumor cells and possible differences between those cells in the handling of the SC-GSL. Liposomes containing the fluorescent SC-GSL C_6-NBD-GalCer were used to treat BLM melanoma cells, 3T3 fibroblasts, and HUVEC endothelial cells, and the lipid fate was followed in living cells for 14 h (Fig. 5A). Shortly after the start of treatment, the fluorescent SC-GSL analogue, C_6-NBD-GalCer, accumulated massively in the plasma membrane of BLM, melanoma cells. After 1 h of incubation fluorescence intensity reached a maximum and remained constant throughout the 14 h time span of the experiment. BLM melanoma cells displayed little intracellular fluorescence before liposome treatment as a cellular background. During the 14 h incubation, intracellular fluorescence increased suggesting lipid internalization and processing. In contrast to BLM tumor cells, 3T3 and HUVEC cell incubations with C_6-NBD-GalCer resulted in lower levels of membrane uptake. For non-tumor cells, C_6-NBD-GalCer fluorescence remained mainly extracellular, most likely liposome associated.

3.6. Native SC-GSL transfer imaged by post-incubation click chemistry

Taking into account that the bulky NBD fluorophore in the SC-GSL could have a tremendous impact on the physicochemical features of the lipid, we synthesized novel SC-GSL analogues as proof of concept for the data obtained with fluorescently C_6-NBD-labeled SC-GSL. To this end, ω-terminal alkyne-GSL analogues (cC8-GlcCer and cC8-GalCer) were synthesized. The transfer and incorporation of SC-GSL into the membrane of tumor vs. non-tumor cells were monitored by click chemistry using the clickable SC-GLS (cSC-GSL) analogues mentioned above. The extension of the transfer and respective incorporation of the lipid analogue into tumor and non-tumor cells was evaluated based on the fluorescence properties of the azide-labeled fluorophore, which labels, after alkyne-azide cycloaddition reaction, the cell-associated c-SC-GSL lipid analogue.

When imaging cC_8-GalCer (Fig. 6A) or cC_8-GlcCer (Fig. 6B) after 2 h at 37 °C, lipids transferred localized into distinct cell compartments according to previous results with fluorescent labeled lipid, C_6-NBD-GalCer, after cell washing. Strikingly, cC_8-GalCer analogue was internalized to a higher extent in tumor cells than in non-tumor cells. In addition, the effect observed is much stronger that the observed with cC_8-GlcCer. Untreated cells were imaged using the same conditions as SC-GSL-treated cells and displayed no Cy3-fluorescent staining.

3.7. Lipid transfer quantification in tumor and non-tumor cells

To quantify SC-GSL insertion into tumor vs. non-tumor cell membranes, we initially performed a set of experiments in HeLa cells in order to find the right experimental conditions. As observed, incorporation into cell membranes is time and concentration dependent (Fig. 7A). After 2 h at 37 °C, SC-GSL levels in cell membranes were higher

Table 1
Liposome characterization.

	Empty-L		Dox-L			
	Size (nm)	pdi	Size (nm)	pdi	Loading (%)	PL recovery (%)
Standard-L	87.5 ± 2.1	0.05 ± 0.02	89.5 ± 1.1	0.06 ± 0.03	88 ± 2.0	68 ± 3.0
C_8-GlcCer-L	89.4 ± 1.4	0.05 ± 0.03	91.3 ± 1.2	0.05 ± 0.04	86 ± 2.0	72 ± 2.0
C_8-GalCer-L	88.4 ± 1.8	0.06 ± 0.01	89.4 ± 1.7	0.07 ± 0.03	85 ± 1.0	73 ± 3.0

More than 3 independent batches were formulated for each formulation and each measurement was performed in triplicate.

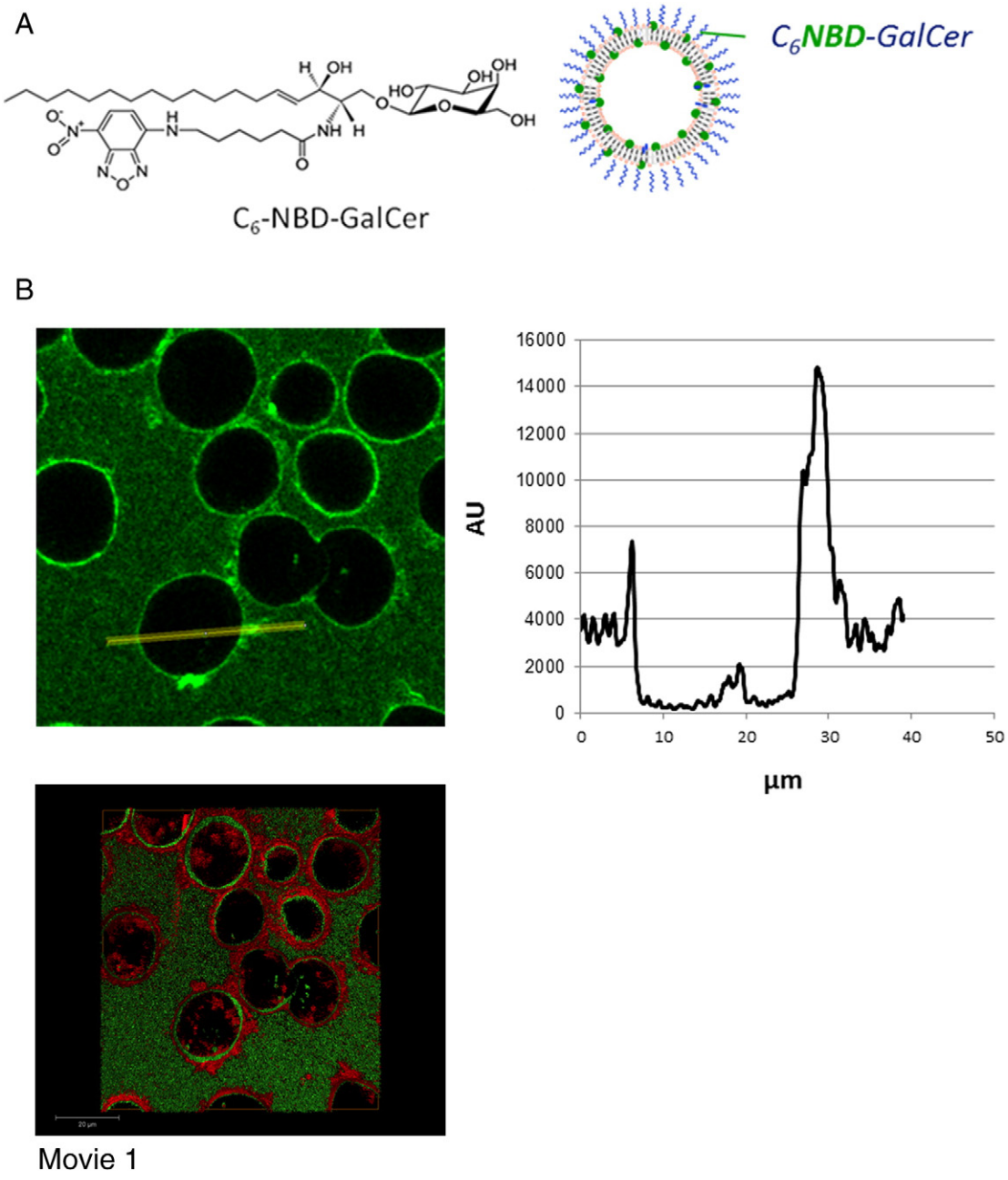

Fig. 2. Live cell confocal microscopy images of SKBR3 human breast carcinoma cells incubated with 20 μM liposomes containing the SC-GSL marker C_6-NBD-GalCer (green) (A) for 2 h at 37 °C. Single cell-lipid transfer quantification was performed by following the fate of C_6-NBD-GalCer fluorescence which increases significantly in the cell membrane and is minor in cytoplasm, referring to a preferential lipid transfer to cellular membrane with higher accumulation in defined plasma membrane areas (B). Movie 1 represents the lipid transfer from the liposomes in suspension (green) and its massive accumulation in the cell membrane (red). Fluorescence intensity was quantified as described in Materials and methods section.

than after 1 h, at same initial SC-GSL concentrations. Increasing SC-GSL concentration (in free form) from 10 to 40 μM, increased cell membrane associated SC-GSL levels (Fig. 7A).

Once the right experimental conditions are found, we next quantify the SC-GSL insertion in tumor and non-tumor cells. Upon treatment of BLM melanoma, MDAMB-231 breast carcinoma and 3T3 fibroblast cells with cSC-GSL (cC_8-GalCer or cC_8-GlcCer) added either in free form (Fig. 7C) or co-inserted in liposome (Fig. 7D) incorporation of the glycosphingolipids into the cells were quantified by TLC and fluorescence imaging. Following lipid extraction, the clickable analogue was subjected to click chemistry reaction, and the amount of SC-GSLs inserted into the different cells was quantified. As a reference, the initial concentration of clickable SC-GSL added to the cells was loaded and the fluorescence value obtained was set to 100%. After normalization, BLM, and MDAMB-231 tumor cells showed higher incorporation of cC_8-GalCer or cC_8-GlcCer than non-tumor fibroblasts ($p < 0.05$) (Fig. 7B). Similarly, when treating cells with liposomes containing cSC-GSL, we observed a preferential incorporation of the lipid into tumor cells in comparison to non-tumor cells ($p < 0.05$) (Fig. 7D). An illustration of the lipid measurement including the peaks of the covered lipid area in different cell lines and respective TLC is represented in Fig. 7C.

3.8. SC-GSLs induce transbilayer redistribution (flip-flop) of pyr-SM in model membranes

Under resting conditions, the diffusion of lipids across lipid bilayers is very slow. Here we studied the effect of SC-GSL on transbilayer lipid redistribution by using model membranes (Fig. 8). LUV's mimicking

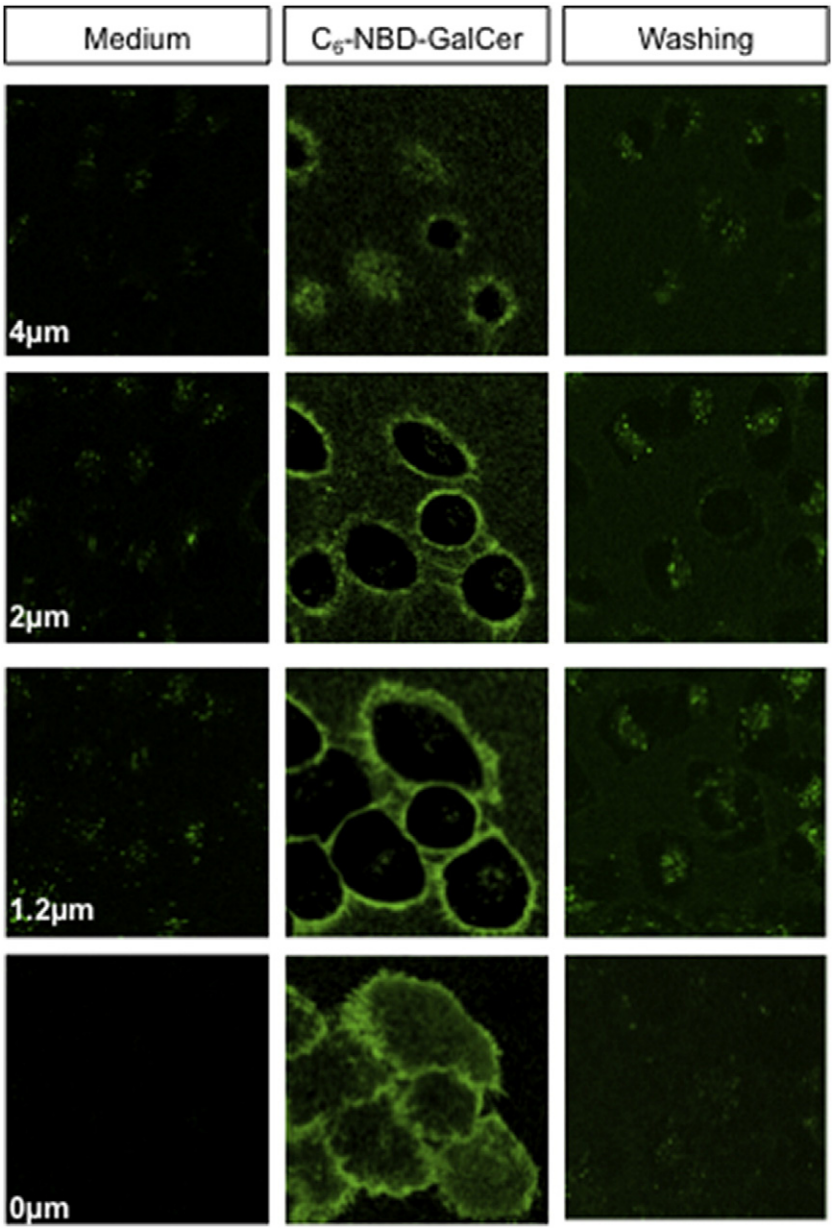

Fig. 3. SC-SGL insertion into cellular membranes is a reversible process. Confocal microscopy imaging of ascending focal planes of BLM, melanoma cells incubated for 2 h at 37 °C with medium (left-panel) or 60 μM C_6-NBD-GalCer liposomes imaged before (central panel) and after washing (right panel).

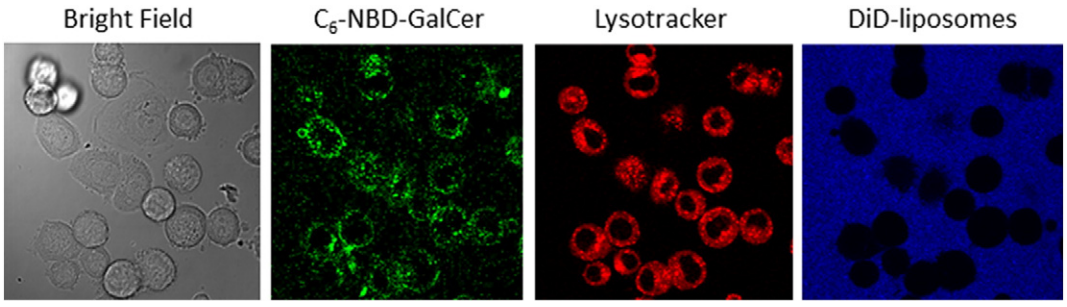

Fig. 4. Live cell confocal microscopy images of SKBR3 human breast carcinoma cells incubated with 60 μM C_6-NBD-GalCer (green) enriched liposomes and the lipophilic tracer DiD marking liposomes bilayer (blue). Colocalization study for C_6-NBD-GalCer and lysotracker was performed incubating cells with red lysotracker for 1 h, washed and further incubated with liposomes containing the SC-GSLs marker C_6-NBD-GalCer. Intracellular colocalization of C_6-NBD-GalCer and lysotracker was minor. Liposomes remained extracellularly, and C_6-NBD-GalCer accumulated at a high extent in the plasma membrane. Cells were imaged with a 63× planachromat oil (n.a. 1.4) objective lens. Representative images of three independent experiments are shown ($n = 3$).

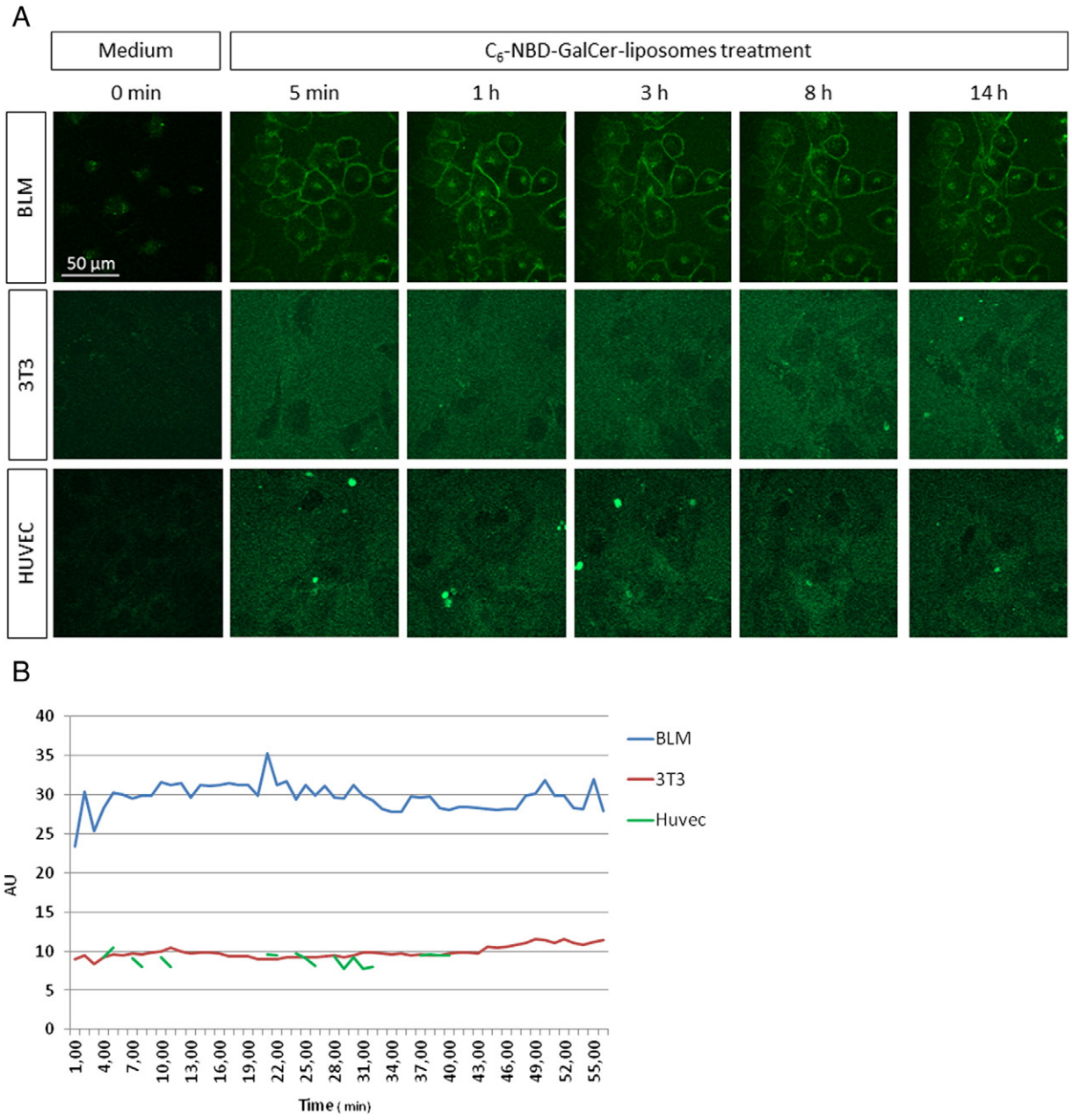

Fig. 5. (A) Time lapse live cell confocal microscopy of BLM melanoma, 3T3 fibroblast and HUVEC endothelial cells before treatment and at different time points after treatment with 60 μM C_6-NBD-GalCer liposomes for a total of 14 h. (B) Intensity of lipid fluorescence was quantified. For HUVEC, broken line represents absence of detected fluorescence. Representative images of three independent experiments are shown (n = 3).

plasma membrane's lipid composition was loaded initially with pyr-SM, which inserts in the outer leaflet [26]. The lipid transbilayer diffusion assay is based on the measurement of the intrinsic properties of the fluorescence pyrene-SM upon redistribution between the outer and inner membrane monolayers. Here, pyr-SM was used to monitor the transbilayer redistribution of the SM in the membrane induced by SC-GSL (C_8-GlcCer or C_8-GalCer) and its clickable analogues (cC_8-GlcCer or cC_8-GalCer). Both lipid analogues showed a similar extent of pyr-SM flip-flop as their natural counterparts. Redistribution of the fluorescent probe from the outer to the inner leaflet led to a decrease of the excimer and an increase of the monomer concentrations. This reflects a SM transbilayer distribution from the outer to the inner leaflet caused by the addition of SC-GSL. Ethanol was used as negative control. Addition of SC-GSL to LUVs caused 30% of SM transbilayer redistribution, 3-fold higher than the control ($p = 0.0109$).

3.9. Formation of aqueous pores

To investigate whether drug-permeable domains formed by SC-GSL represent physical aqueous pores, model membranes encapsulating hydrophilic low molecular weight compounds were investigated for possible SC-GSL-induced permeability. Membrane passage of hydrophilic ANTS–DPX complexes upon incubation with SC-GSL-liposomes was studied. These water-soluble complexes exist as a non-fluorescent complex when entrapped in the LUV's core. Upon the formation of a hydrophilic pore, vesicle efflux occurs, causing dilution of the complex and subsequent ANTS–DPX dissociation, which can be assessed by measuring ANTS fluorescence (Fig. 9). 100% leakage of ANTS–DPX was set by total disruption of LUV's in the presence of detergent. Incubation of C_8-GalCer or C_8-GlcCer liposomes with ANTS–DPX entrapped in LUVs did not display changes in fluorescence demonstrating that ANTS

remained associated to DPX in the vesicle core. As positive control, tetanolysin, a cholesterol-binding dependent toxin was used to create pores in the bilayer. Based on these results, transient pore formation induced by SC-GSL is excluded as a possible mechanism used by SC-GSL to boost drug binding and uptake in cells.

3.10. Influence of temperature on function of SC-GSL as intracellular drug uptake enhancers

To address the mechanism of SC-GSL as drug uptake enhancers, SC-GSL enriched liposomes containing Dox were used to treat MDAMB-231 breast carcinoma and BLM melanoma cells. Using the autofluorescent properties of Dox, intracellular drug uptake was followed by confocal microscopy and drug uptake levels of SC-GSL-enriched liposomes (GalCer-DoxL) were compared to standard liposomes (Dox-L) without SC-GSL and free drug. Cellular incubation at 4 °C causes a more laterally ordered lipid bilayer and increases cell membrane rigidity [34]. It also inhibits energy-dependent drug transport across the cell membrane. Dox was imaged in MDAMB-231 or BLM cells by live cell confocal microscopy after 2 h of incubation at 4 °C before and after washing (Fig. 10 left panels). After imaging, cells were further incubated for 2 h at 37 °C, and then imaging before and after washing was performed (Fig. 10 right panels).

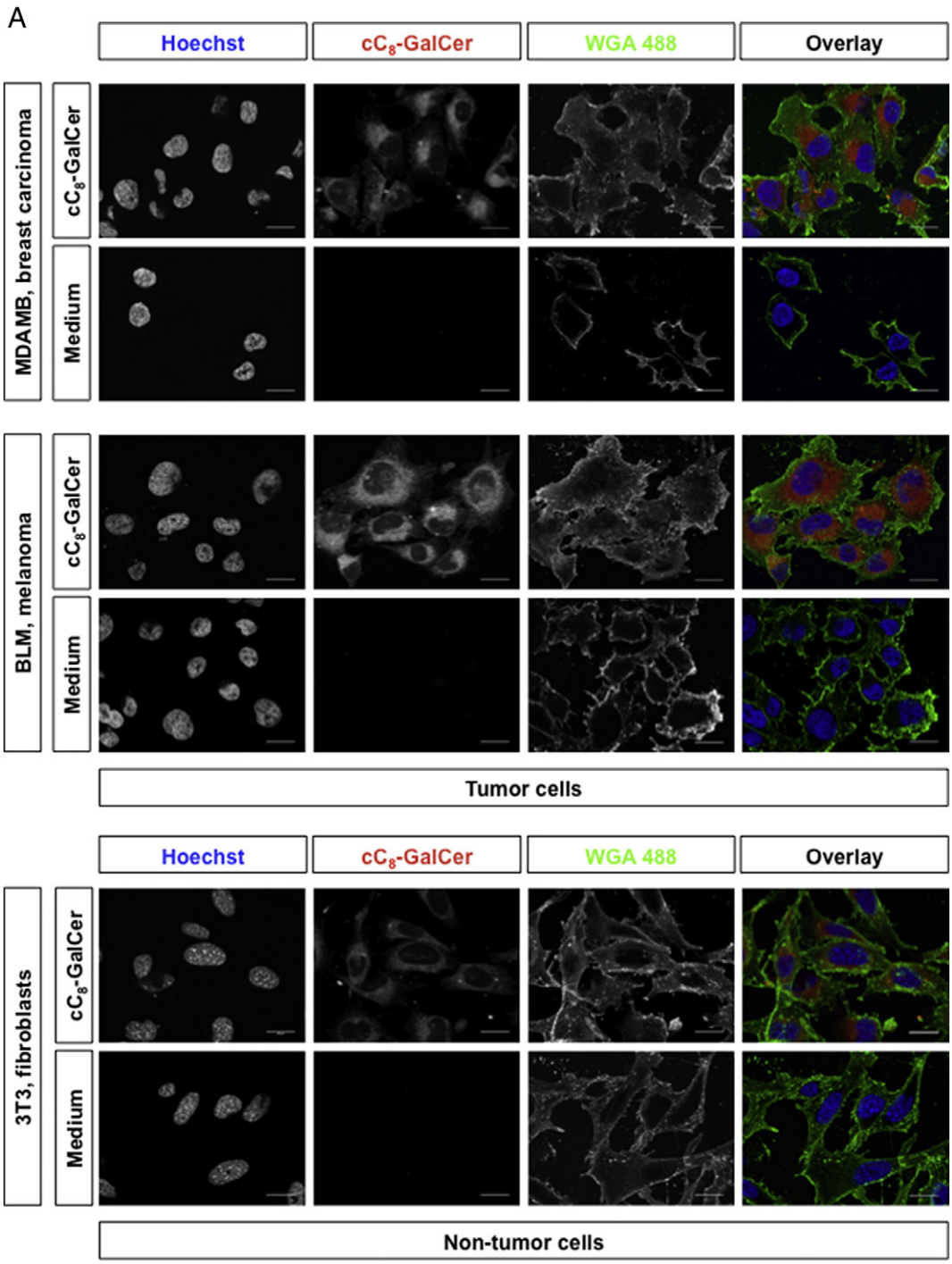

Fig. 6. Confocal imaging of fluorescently labeled cSC-GSL incorporation into tumor cells (BLM melanoma and MDAMB-231 breast carcinoma) and non-tumor cells (3T3 fibroblasts). Cells treated with 10 μM of either cC_8-GalCer (A) or cC_8-GlcCer (B) for 2 h were fixed and subjected to click reaction with Cy3-azide (red). Nuclear and plasma membrane staining were performed with Hoechst (blue) and WGA 488 (green), respectively. Representative images of three independent experiments are shown (n = 3).

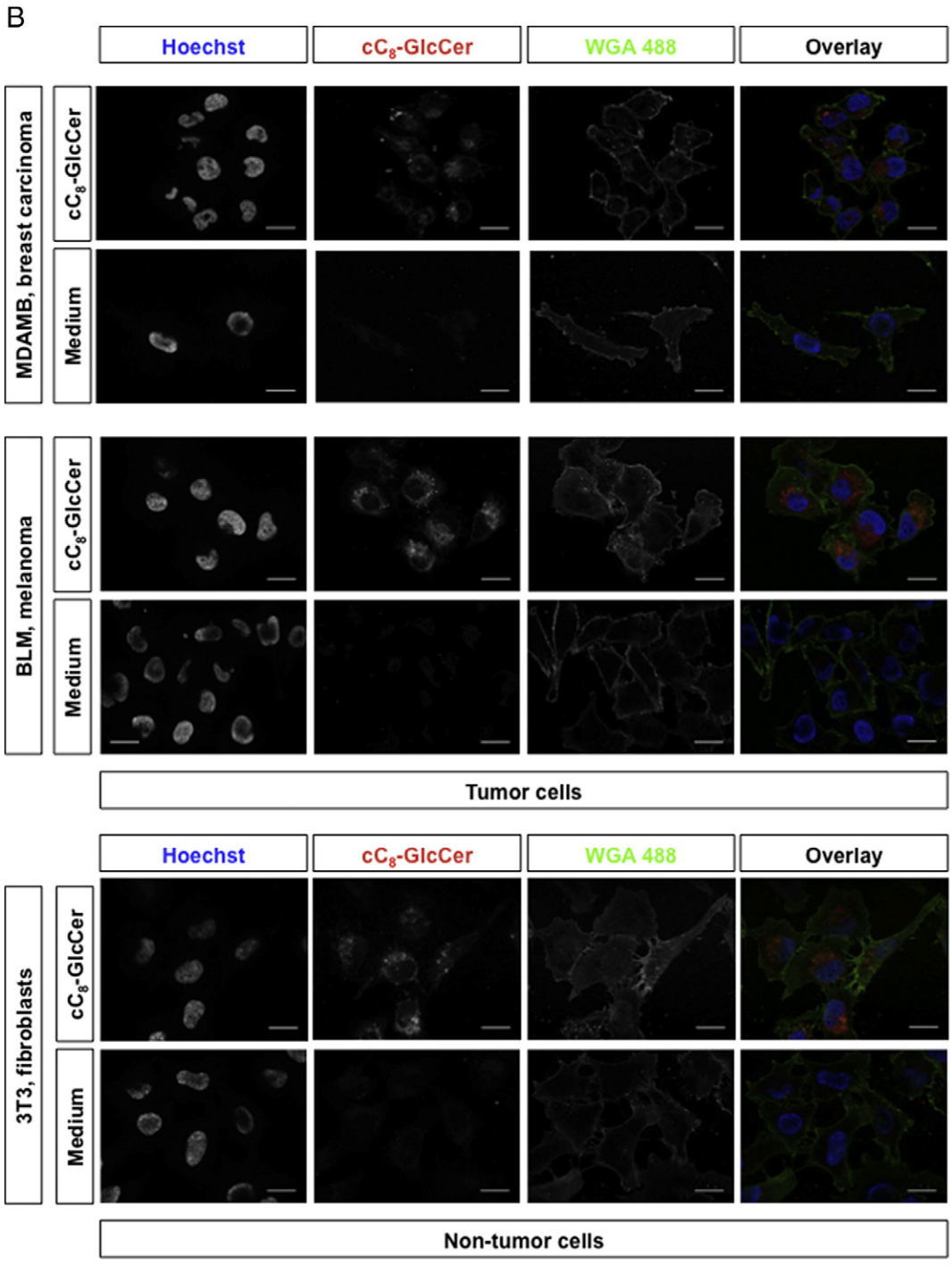

Fig. 6 (*continued*).

No cellular uptake of free Dox was observed in MDAMB-231 carcinoma and BLM melanoma cells at 4 °C. A signal from free Dox is visible as a reddish background in the extracellular space. More abundant Dox fluorescence is found to be associated with MDAMB 231 and BLM cells are incubated with SC-GSL enriched Dox-liposomes (GalCer-L) at 4 °C. Treatment with standard liposomes at 4 °C results in hardly detectable intracellular drug levels, and Dox signal is almost entirely lost after washing, indicating that the fluorescent signal before washing resulted from membrane-associated drug. After an additional incubation at 37 °C for 2 h (third column), both cell lines showed nuclear uptake of free Dox. Most of Dox signals remain after washing confirming intracellular presence, especially in the nucleus, whereas some cytoplasmic or membrane-associated Dox is also removed upon washing. After the treatment with SC-GSL-enriched liposomes for 2 h at 4 °C and 2 h at 37 °C, Dox is found to be intracellular in the nucleus as well as cytoplasmic and membrane-associated. Following washing, the cytoplasmic/membrane-associated drug fraction is almost entirely removed from cells, and intracellular Dox is naturally directed to the nucleus where it exerts its cytotoxic action. At 37 °C, when cells were treated with GalCer-DoxL, Dox reached the nucleus where it is retained. For standard liposomes, cytoplasmic, nuclear Dox uptake is minimal and is mainly cytoplasmic or membrane bound.

Finally, the effect of SC-GSL on intracellular Dox uptake was quantified by flow cytometry in tumor BLM, melanoma and non-tumor 3T3

fibroblasts. Both C_8-GlcCer or C_8-GalCer enriched liposomes showed enhanced intracellular drug levels in comparison to standard liposomes and preferentially in tumor cells (**$p < 0.01$) (Supplemental Fig. 2).

4. Discussion and conclusion

Our initial working hypothesis is based on a spontaneous transfer of the SC-GSL from the liposomal bilayer to the cell membrane, leading to cell membrane permeability modifications and subsequent enhancing of intracellular amphiphilic drug influx. This mechanism suggests a novel possible way to improve therapeutic efficacy of applied cytostatic drug in cancer treatment [15,16,18]. Here, we investigated the molecular mechanism of action underlying liposomal SC-GSL as cellular drug uptake enhancer.

In this study we were able to demonstrate that upon cellular contact SC-GSLs are spontaneously transferred from the liposomal bilayer to the plasma membrane, most likely into the exoplasmatic leaflet (Fig. 2, Supplemental Fig. 1) where Dox membrane interaction and transmembrane transport are facilitated [30]. To validate the results obtained with the fluorescent analogue NBD-GalCer (Fig. 2A), which fluorophore is known to change the biophysical, trafficking and metabolical features of the lipid in some cases, we designed and synthesized novel SC-GSL analogues. These new molecules have a ω-terminal alkyne for click chemistry reaction with a fluorescently labeled azide. Using these novel cSC-GSLs (cC_8-GlcCer or cC_8-GalCer), it was possible to follow the fate of the lipid without interfering with its original and native structure. SC-GSL transfer occurred mainly in intracellular compartments at higher extension in tumor cells, and its intracellular accumulation was found to be concentration dependent (Figs. 6 and 7). The fluorescently labeled SC-GSL analogue C_6-NBD-GalCer inserted in the liposomal bilayer (Fig. 2A) is transferred and re-distributed throughout the plasma membrane with seemingly increased levels in filopodia or lamellopodia like cellular protrusions (Fig. 2B, Movie 1). Such particular structures were only observed in cells treated with SC-GSL enriched liposomes, confirming a close contact between particles and cells, which supports short-chain GSL transfer and subsequently plasma membrane structure destabilization (Supplemental Fig. 1). Biomembranes are non-equilibrium structures, in which lipid asymmetry is maintained by active transbilayer lipid transport [31,32]. When lipid transfer occurs in one direction, it is naturally compensated by the simultaneous transfer of (the same or) other lipids in the reciprocal direction so that mass conservation in each monolayer is maintained. The opposite situation,

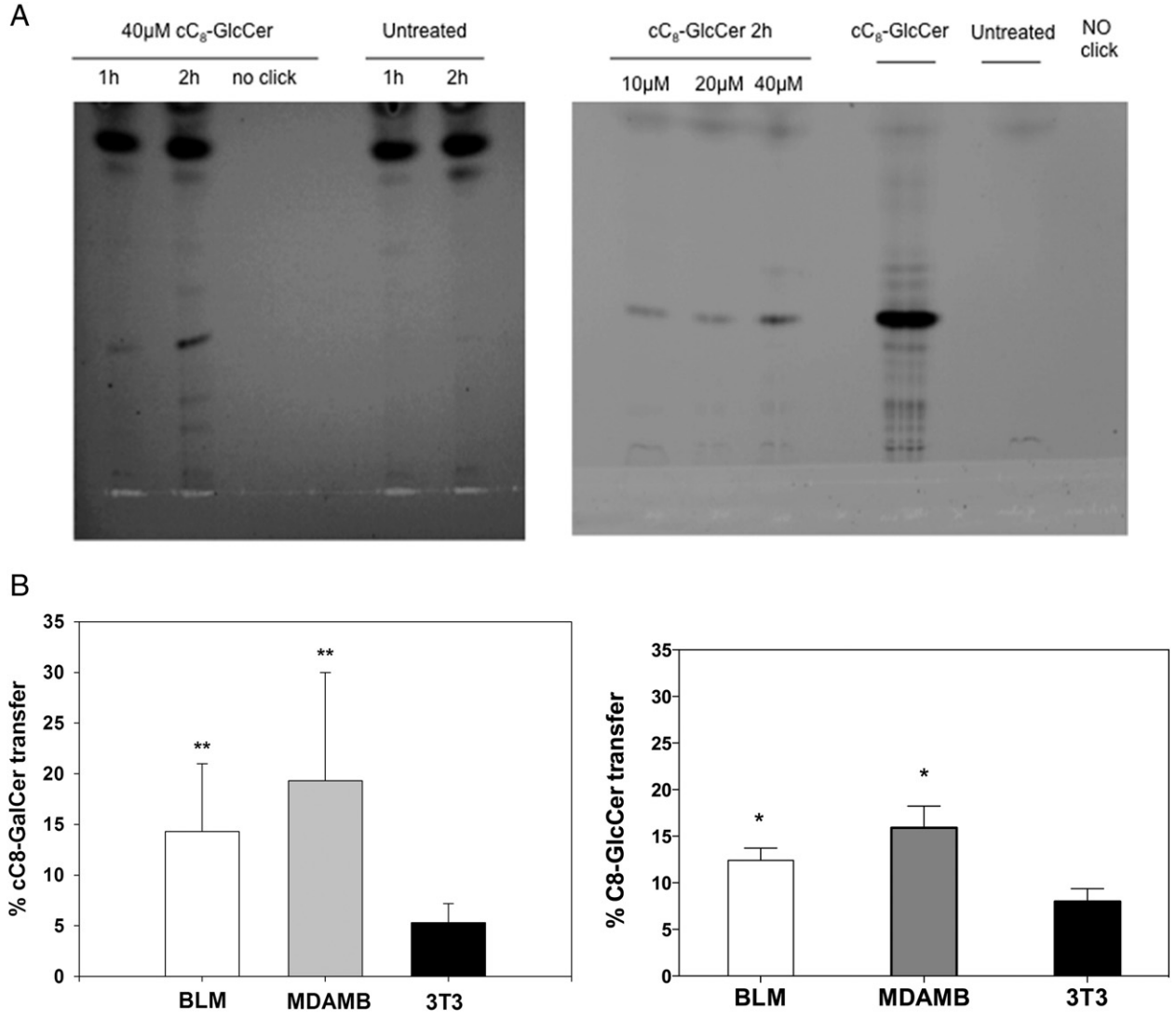

Fig. 7. Lipid transfer quantification in tumor versus non-tumor cells. (A) cC_8-GlcCer lipid analogue insertion is concentration and exposure time dependent. (B) cC_8-GalCer or cC_8-GlcCer lipid analogue insertion into plasma membranes was quantified by click chemistry. Lipid transfer in tumor cells was significantly (*)($p < 0.05$) or very significantly (**)($p < 0.01$) higher than in non-tumor cells. SC-GSL transfer to the plasma membrane was quantified by TLC in free form (C) or liposome co-inserted (D). Control was set as 100% of initial lipid amount. Six independent experiments were performed. Results of unpaired, two-tailed *t*-test are given: *$p \leq 0.05$ or **$p < 0.01$ in comparison to 3T3, fibroblasts. Twin numbers under the lipid extraction running correspond to duplicates of the experiments.

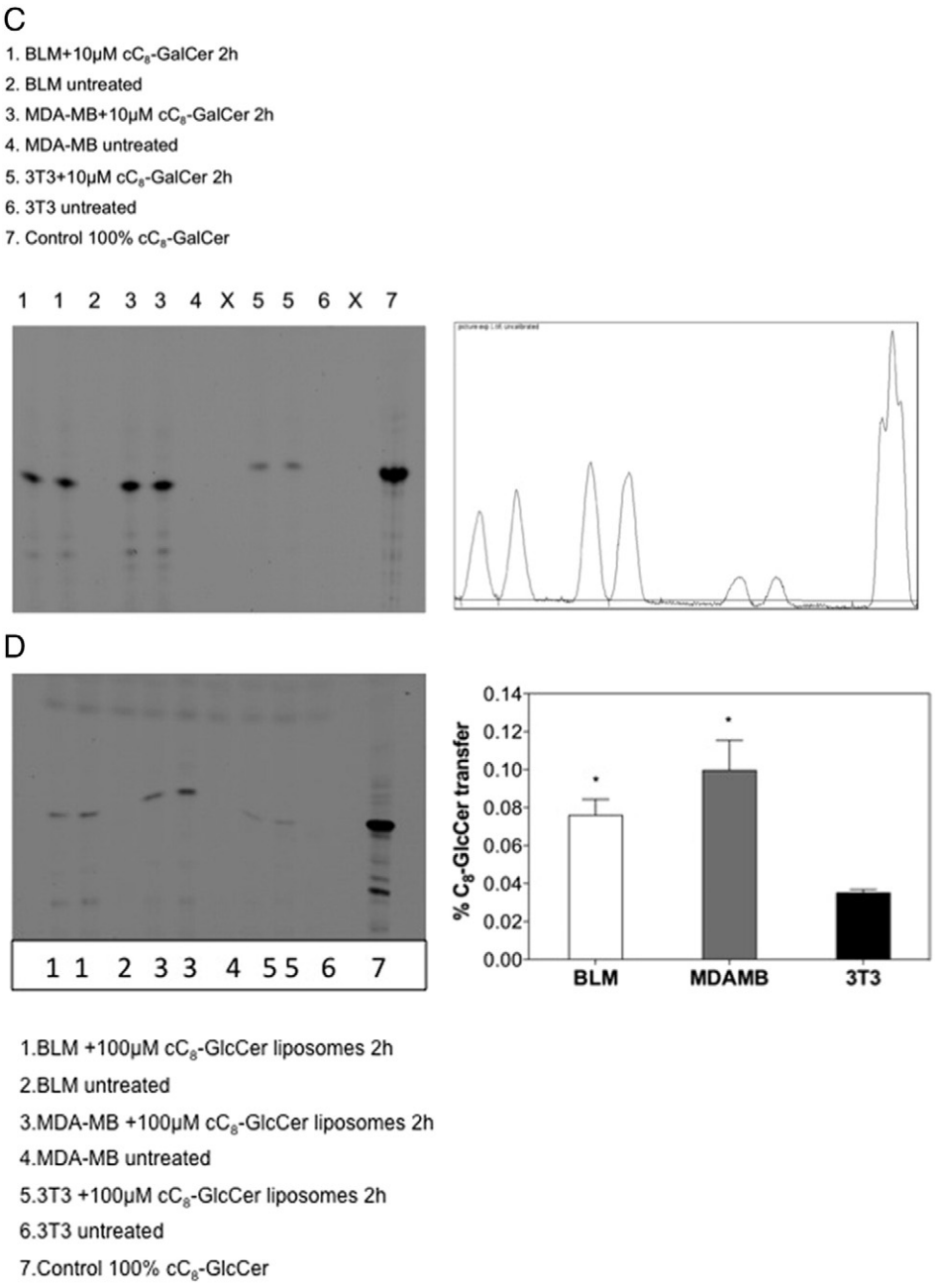

Fig. 7 (*continued*).

namely the net transfer of mass (lipid molecules), would lead to higher lateral pressure and bilayer collapsing. It is also known that the maintenance of membrane asymmetry in the resting state is energy dependent, and that flip-flop of lipids cannot occur by itself [32]. Transbilayer lipid motion triggered by external agents has been shown only for long-chain ceramides [20]. Here, we have demonstrated a highly efficient transbilayer lipid movement or flip-flop by external glycosylated short-chain glycosylceramides, C_8-GlcCer or C_8-GalCer (Fig. 8). Moreover, the transbilayer lipid movement from the outer to the inner leaflet measured in this work with SC-GSL is higher than the previously described with short-chain ceramides (C_6 or C_2-ceramide) by our group [20]. This points to a different molecular mechanism of action for SC-GSLs, where the sugar head group could play a major role in the formation and stabilization of transitory membrane nanopore, which facilitates lipid flip-flop and cellular drug uptake. Finally, the ability of cC_8-Glc-Cer and cC_8-GalCer to induce a similar extent of flip-flop in model membranes compared to natural ones proves that the physicochemical properties of the analogues are very close to their natural counterparts (Fig. 8).

External addition of SC-GSL like C_8-GlcCer or C_8-GalCer [33,34] might induce membrane lipid rearrangement, when self-associating or interacting with natural lipids (i.e. cholesterol, sphingolipids) present in the outer leaflet of the plasma membrane facilitating lipid microdomain formation and membrane permeability. It has been described that N-acyl long chain (more than 12 °C) ceramides but not N-acyl short-chain ceramides were able to induce the formation of stable lipid microdomains [35]. Here, possible pore domain formation, similar to the described with ceramides, induced by SC-GSL transfer to model membranes was also studied (Fig. 9). The results obtained did not show a leakage of hydrophilic compounds, confirming previously reported data by co-workers in cellular studies [14], where it was shown that C_6-SM does not increase membrane permeability of a

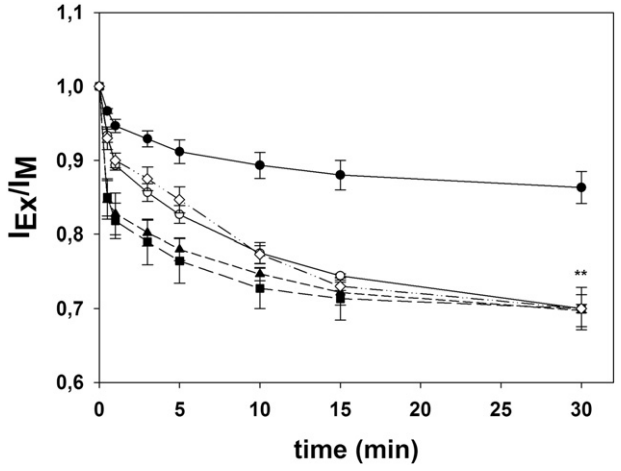

Fig. 8. Short-chain GSLs induced transbilayer movement of pyr-SM in plasma membrane like LUVs. The original lipid concentration was 300 μM. The following additions were made to 1 ml of the LUV suspension at time 0: 15 μM C_8-GlcCer in 2 μl of ethanol (■), 15 μM C_8-GalCer in 2 μl ethanol (▲), 15 μM cC_8-GlcCer in 2 μl ethanol (○), 15 μM cC_8-GalCer in 2 μl ethanol ( ), and 2 μl ethanol (●). Average values ± SD (n = 3). Results of unpaired, two-tailed *t*-test are given: $^{**}p \leq 0.01$.

hydrophilic marker (AF488-hydrazine) or a cytosolic protein (LDH) [15]. Possibly, SC-GSL induces the rearrangement of the cell membrane enhancing intracellular drug uptake by processes that do not include aqueous pore domain formation.

It has been described that a sugar moiety in the polar head group weakens intermolecular interactions by reducing packing efficiency [36]. In the case of glycosylsphingolipids, such as C_8-GlcCer and C_8-GalCer (containing relatively small polar head groups) the increase of molecular order acquired by close packing is unfavorable because it cannot be compensated by release of enough molecules of water from the polar head group hydration shell [36]. Partly, this supports the rearrangement of the plasma membrane structure by the transfer of SC-GSLs (Fig. 8) with increased permeability to drug traversal (Fig. 10, Supplemental Fig. 2). SC-GSL insertion in the cell membrane might lower packing density, promoting Dox insertion and Dox–SC-GSL interaction [17] or enhancing exposure Dox to binding lipids (e.g. PE) in the plasma membrane improving intracellular drug uptake [37].

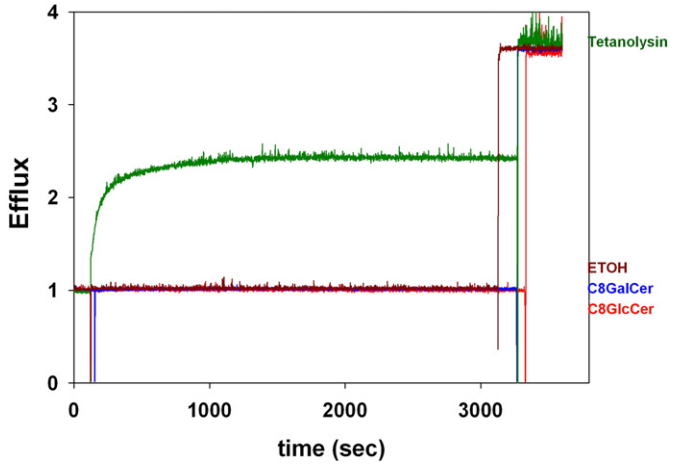

Fig. 9. Time course of SC-GSLs induced efflux of ANTS/DPX. 15 μM of C_8-GalCer (blue) or C_8-GlcCer (red) was externally added to freshly prepared plasma membrane like LUVs (300 μM), and ANTS/DPX efflux monitored over time. Ethanol (2 μl) and tetanolysin (10 ng) were used as negative and positive controls, respectively. Representative image of three independent experiments are shown (n = 3).

SC-GSL-plasma membrane transfer was found to be reversible as observed after extensive cell washing (Fig. 3). These findings suggest that SC-GSLs accumulate to a large extent in the outer leaflet of the PM. Whereas lipid transfer to the plasma membrane occurred substantially, this occurred without intracellular uptake of the liposomes (Fig. 4) which confirms previous data on enhanced drug uptake by non-fluorescently labeled-SC-GSL enriched liposomes containing Dox in MCF-7 breast carcinoma cell line [18]. Besides a massive transfer to the plasma membrane (Fig. 2B, Movie 1 — red) part of the lipid remained associated with the liposomal bilayer (Movie 1 — green). The transfer phenomenon occurs from filled to empty SC-GSL membranes, a concentration gradient that requires only SC-GSL enriched liposome versus plasma membrane contact. Although massive membrane accumulation was observed for prolonged periods (Fig. 3), intracellular presence of C_6-NBD-GalCer was found although in a minor extent, especially after extensive washing, which removed the majority of membrane-associated SC-GSLs (Figs. 3 and 4). Live cell imaging with C_6-NBD-GalCer (Fig. 5) and click chemistry lipid quantification (Fig. 7) in free and liposomal forms of tumor and non-tumor cells demonstrated a preferential transfer and incorporation of SC-GSLs into tumor cell membranes (Fig. 7B, C, D). This result confirms earlier observations showing that the drug uptake enhancing properties of SC-GSLs and subsequent induction of cytotoxicity are much more specific for various tumor cell lines and much less for normal cells [15,16,18,29]. By preferentially targeting the tumor cell membrane (Figs. 5, 7) and modulating its permeability to drug uptake (Fig. 10, Supplemental Fig. 2) [18,29], SC-GSLs represent a promising possibility to improve chemotherapy efficacy. In addition, live cell imaging and co-staining with lysotracker confirmed minor lysosomal localization of C_6-NBD-GalCer (Fig. 4). Lipidome analysis of tumor and non-tumor cells shows a distinguished phospholipid pattern mainly at the level of phosphatidylcholine (PC), phosphatidylethanolamine (PE), phosphatidylserine, sphingomyelin (SM) and phosphatidylinositol (PI) [38]. Differences in phospholipid patterns are described to decrease membrane permeability of tumor cells by an increased rigidity and promote tumor progression [17,38]. Recently, it has been reported that faster-proliferating cells modulate and rearrange their lipidome [39] supporting the differential phospholipid composition between tumor and non-tumor cells. In addition, lower cholesterol levels are described to increase membrane fluidity in tumor cells [17,38]. The lipidome of tumor cells is also associated with multidrug resistance phenomenon influencing the ability of tumor cells to respond to chemotherapy [40]. Likely the specific cellular lipidome determines the affinity for SC-GSL membrane insertion and subsequently causes enhanced drug uptake specifically in tumor cells (Figs. 5, 7, Supplemental Fig. 2).

The process by which Dox normally crosses the plasma membrane involves spontaneous adsorption by insertion of the molecule's hydrophobic anthraquinone into the exoplasmic leaflet of the lipid bilayer, followed by an energetically unfavorable flip-flop of the drugs' hydrophilic sugar moiety between the outer and the inner membrane leaflets. At physiological conditions, this flip-flop is extremely slow with a half-life of 0.7 min [30]. The cellular uptake of free Dox at 4 °C (Fig. 10) is therefore virtually impossible for thermodynamic reasons. The marginal signal of free Dox at 4 °C in Fig. 10 hence results from membrane-associated Dox molecules, but Dox transmembrane transport does not occur and no uptake of free Dox occurred at 4 °C neither in MDAMB 231 nor in BLM tumor cells. Comparing the results from Figs. 4 with 10 reveals that Dox fluorescence in Fig. 10 is originated from Dox in the free and not liposomal form since liposomes are not taken up and so remain extracellular. Membrane-associated Dox can easily be washed away, explaining complete loss of fluorescent signal after washing cells treated with free Dox at 4 °C. In addition cells treated with Dox in form of SC-GSL enriched liposomes show an intense signal for membrane-associated Dox even at 4 °C with the transmembrane transport blocked. Washing reveals that Dox is mostly membrane co-associated with SC-GSL. At 4 °C, the presence of SC-GSL in the liposome

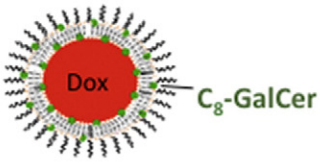

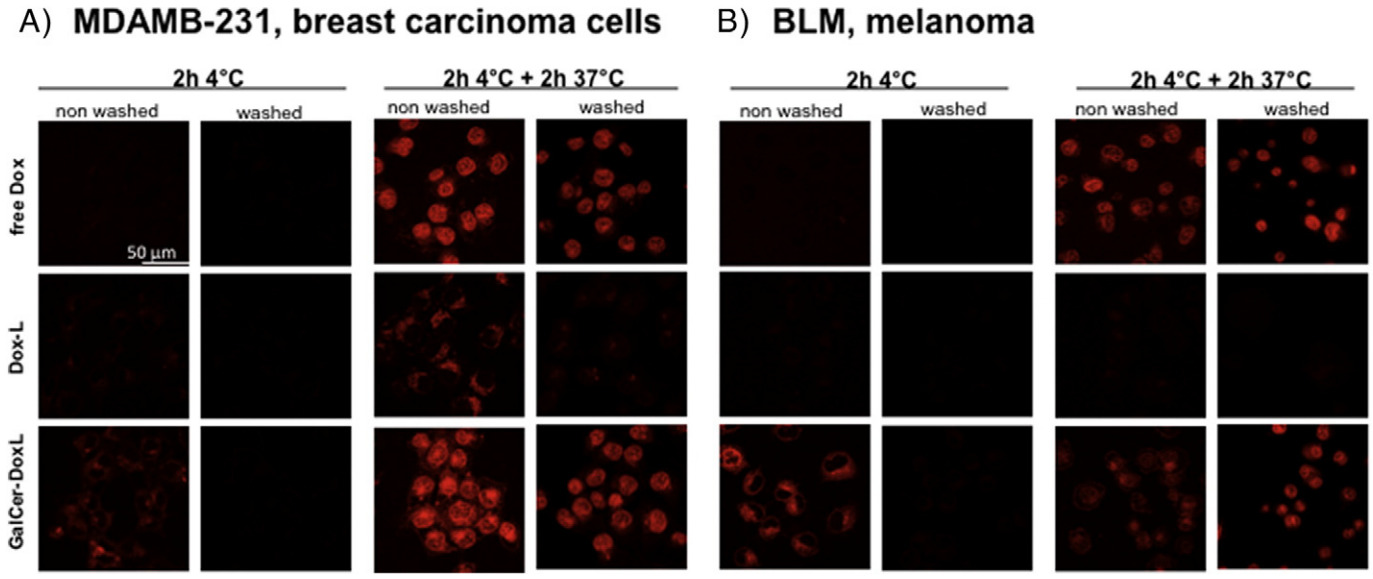

Fig. 10. Temperature-dependent intracellular Dox uptake in MDAMB-231 carcinoma cells (A) and BLM melanoma cells (B). Imaging of cells treated with either 40 μM of GalCer-DoxL or Dox-L or free Dox incubated at 4 °C for 2 h or at 4 °C for 2 h and immediately at 37 °C for 2 h were taken before (left panel) and after washing (right panel), respectively. Red fluorescence represents Dox. Representative image of three independent experiments are shown (n = 3).

membrane greatly enhances Dox–plasma membrane interaction, compared to non-enriched liposomes. This suggests that at 4 °C, SC-GSLs exert their effect on the outer membrane leaflet. At 4 °C, the reduced membrane fluidity leads to stabilization of lipid microdomains, blocking intracellular transport and perhaps slowing down the flip-flop process. After additional incubation at 37 °C for 2 h, of MDAMB 231 or BLM cells, intracellular uptake of Dox delivered as free drug was comparable to Dox delivered from SC-GSL enriched liposomes, whereas uptake of non-enriched liposomes is marginal (Fig. 10, Supplemental Fig. 2). Here, we conclude that SC-GSLs exert their effect on the outer membrane leaflet, where they enhance the Dox–membrane influx by a biophysical process and consequently facilitate Dox membrane traversal. Considering the easy washing of Dox molecules at 4 °C and of SC-GSL molecules as observed in Fig. 3, we may speculate on the association of Dox molecules to SC-GSL at the level of the outer leaflet without interference with cellular mechanisms. This is supported by modeling experiments by Van Hell and coworkers, who reported molecular assembly of SC-GSL and Dox when the latter associates to the hydrophobic core of the bilayer [17].

In summary, important insights into the mechanism by which SC-GSL enhance drug uptake are described. SC-GSL can transfer spontaneously to the plasma membrane preferentially in tumor cells modulating plasma membrane permeability to cytostatics drugs, therefore enhancing its influx and efficacy. Moreover, membrane-restructuring effects within the plasma membrane induced by SC-GSL were determined as the driven role for enhanced intracellular drug influx. This mechanism, besides representing an exciting tool to improve the specific targeting of tumoral cells, might also reverse chemotherapy resistance.

Supplementary data to this article can be found online at http://dx.doi.org/10.1016/j.bbamem.2015.04.011.

Transparency document

The Transparency document associated with this article can be found, in the online version.

Acknowledgements

This work was supported in part by grants from the Spanish Ministry of Economy BFU2012-33103 (to: FXC), the Basque Government IT852-13 (to: FXC) and the Dutch Cancer Society (to: GAK) (NKI 2008-4113). D.C. acknowledges the support from Fundación Biofísica Bizkaia. The authors thank the OIC for their assistance.

References

[1] A. Gabizon, H. Shmeeda, Y. Barenholz, Pharmacokinetics of pegylated liposomal doxorubicin: review of animal and human studies, Clin. Pharmacokinet. 2 (5) (2003) 419–436.
[2] T.M. Allen, P.R. Cullis, Liposomal drug delivery systems: from concept to clinical applications, Adv. Drug Deliv. Rev. 65 (2013) 36–48.
[3] G.A. Koning, G.C. Krijger, Targeted multifunctional lipid-based nanocarriers for image-guided drug delivery, Anti Cancer Agents Med Chem. 7 (4) (2007) 425–440.
[4] A.A. Gabizon, Pegylated liposomal doxorubicin: metamorphosis of an old drug into a new form of chemotherapy, Cancer Invest. 19 (4) (2001) 424–436.
[5] M.E. O'Brien, N. Wigler, M. Inbar, R. Rosso, E. Grischke, A. Santoro, R. Catane, D.G. Kieback, P. Tomczak, S.P. Ackland, F. Orlandi, L. Mellars, L. Alland, C. Tendler, CAELYX Breast Cancer Study Group, Reduced cardiotoxicity and comparable efficacy in a phase III trial of pegylated liposomal doxorubicin HCl (CAELYX/Doxil) versus conventional doxorubicin for first-line treatment of metastatic breast cancer, Ann. Oncol. 15 (2004) 440–449.
[6] D.W. Northfelt, B.J. Dezube, J.A. Thommes, B.J. Miller, M.A. Fischl, A. Friedman-Kien, L.D. Kaplan, C. Du Mond, R.D. Mamelok, D.H. Henry, Pegylated-liposomal doxorubicin versus doxorubicin, bleomycin, and vincristine in the treatment of AIDS-related Kaposi's sarcoma: results of a randomized phase III clinical trial, J. Clin. Oncol. 16 (1998) 2445–2451.

[7] T. Tejada-Berges, C.O. Granai, M. Gordinier, W. Gajewski, Caelyx/Doxil for the treatment of metastatic ovarian and breast cancer, Expert. Rev. Anticancer. Ther. 2 (2) (2002) 143–150.
[8] M.A. Hussein, K.C. Anderson, Role of liposomal anthracyclines in the treatment of multiple myeloma, Semin. Oncol. 31 (2004) 147–160.
[9] D.S. Alberts, F.M. Muggia, J. Carmichael, E.P. Winer, M. Jahanzeb, A.P. Venook, K.M. Skubitz, E. Rivera, J.A. Sparano, N.J. DiBella, S.J. Stewart, J.J. Kavanagh, A.A. Gabizon, Efficacy and safety of liposomal anthracyclines in phase I/II clinical trials, Semin. Oncol. 31 (2004) 53–90.
[10] H. Maeda, H. Nakamura, J. Fang, The EPR effect for macromolecular drug delivery to solid tumors: Improvement of tumor uptake, lowering of systemic toxicity, and distinct tumor imaging in vivo, Adv. Drug Deliv. Rev. 65 (2013) 71–79.
[11] K.M. Laginha, S. Verwoert, G.J. Charrois, T.M. Allen, Determination of doxorubicin levels in whole tumor and tumor nuclei in murine breast cancer tumors, Clin. Cancer Res. 11 (19 Pt 1) (2005) 6944–6949.
[12] A.L. Seynhaeve, S. Hoving, D. Schipper, C.E. Vermeulen, Ga de Wiel-Ambagtsheer, S.T. van Tiel, A.M. Eggermont, T.L. Ten Hagen, Tumor necrosis factor alpha mediates homogeneous distribution of liposomes in murine melanoma that contributes to a better tumor response, Cancer Res. 67 (19) (2007) 9455–9462.
[13] K.M. Laginha, E.H. Moase, N. Yu, A. Huang, T.M. Allen, Bioavailability and therapeutic efficacy of HER2 scFv-targeted liposomal doxorubicin in a murine model of HER2-overexpressing breast cancer, J. Drug Target. 16 (7) (2008) 605–610.
[14] R.J. Veldman, S. Zerp, W.J. van Blitterswijk, M. Verheij, N-hexanoyl-sphingomyelin potentiates in vitro doxorubicin cytotoxicity by enhancing its cellular influx, Br. J. Cancer 90 (4) (2004) 917–925.
[15] R.J. Veldman, G.A. Koning, A. van Hell, S. Zerp, S.R. Vink, G. Storm, M. Verheij, W.J. van Blitterswijk, Coformulated N-octanoyl-glucosylceramide improves cellular delivery and cytotoxicity of liposomal doxorubicin, J. Pharmacol. Exp. Ther. 315 (2) (2005) 704–710.
[16] M. van Lummel, W.J. van Blitterswijk, S.R. Vink, R.J. Veldman, M.A. van der Valk, D. Schipper, B.M. Dicheva, A.M. Eggermont, T.L. ten Hagen, M. Verheij, G.A. Koning, Enriching lipid nanovesicles with short-chain glucosylceramide improves doxorubicin delivery and efficacy in solid tumors, FASEB J. 25 (1) (2011) 280–289.
[17] A.J. van Hell, M.N. Melo, W.J. van Blitterswijk, D.M. Gueth, T.M. Braumuller, L.R. Pedrosa, J.Y. Song, S.J. Marrink, G.A. Koning, J. Jonkers, M. Verheij, Defined lipid analogues induce transient channels to facilitate drug-membrane traversal and circumvent cancer therapy resistance, Sci. Rep. 3 (2013) 1949.
[18] L.R. Pedrosa, A. van Hell, R. Süss, W.J. van Blitterswijk, A.L. Seynhaeve, W.A. van Cappellen, A.M. Eggermont, T.L. ten Hagen, M. Verheij, G.A. Koning, Improving intracellular doxorubicin delivery through nanoliposomes equipped with selective tumor cell membrane permeabilizing short-chain sphingolipids, Pharm. Res. 30 (7) (2013) 1883–1895.
[19] F.X. Contreras, A.V. Villar, A. Alonso, R.N. Kolesnick, F.M. Goñi, Sphingomyelinase activity causes transbilayer lipid translocation in model and cell membranes, J. Biol. Chem. 278 (39) (2003) 37169–37174.
[20] F.X. Contreras, G. Basañez, A. Alonso, A. Herrmann, F.M. Goñi, Asymmetric addition of ceramides but not dihydroceramides promotes transbilayer (flip-flop) lipid motion in membranes, Biophys. J. 88 (1) (2005) 348–359.
[21] L.J. Siskind, M. Colombini, The lipids C2- and C16-ceramide form large stable channels implications for apoptosis, J. Biol. Chem. 275 (49) (2000) 38640–38644.
[22] S. Samanta, J. Stiban, T.K. Maugel, M. Colombini, Visualization of ceramide channels by transmission electron microscopy, Biochim. Biophys. Acta 1808 (4) (2011) 1196–1201.
[23] J. Sot, L.A. Bagatolli, F.M. Goñi, A. Alonso, Detergent-resistant, ceramide-enriched domains in sphingomyelin/ceramide bilayers, Biophys. J. 90 (3) (2006) 903–914.
[24] F.X. Contreras, A.M. Ernst, P. Haberkant, P. Björkholm, E. Lindahl, B. Gönen, C. Tischer, A. Elofsson, G. von Heijne, C. Thiele, R. Pepperkok, F. Wieland, B. Brügger, Nature 481 (7382) (2012) 525–529.
[25] C. Thiele, C. Papan, D. Hoelper, K. Kusserow, A. Gaebler, M. Schoene, K. Piotrowitz, D. Lohmann, J. Spandl, A. Stevanovic, A. Shevchenko, L. Kuerschner, Tracing fatty acid metabolism by click chemistry, ACS Chem. Biol. 7 (12) (2012) 2004–2011.
[26] K. Temmerman, W. Nickel, A novel flow cytometric assay to quantify interactions between proteins and membrane lipids, J. Lipid Res. 50 (6) (2009) 1245–1254.
[27] P. Müller, S. Schiller, T. Wieprecht, M. Dathe, A. Herrmann, Continuous measurement of rapid transbilayer movement of a pyrene-labeled phospholipid analogue, Chem. Phys. Lipids 106 (1) (2000) 89–99.
[28] H. Ellens, J. Bentz, F.C. Szoka, H+- and Ca^{2+}-induced fusion and destabilization of liposomes, Biochemistry 24 (13) (1985) 3099–3106.
[29] L.R. Pedrosa, T.L. Ten Hagen, R. Süss, A. van Hell, A.M. Eggermont, M. Verheij, G.A. Koning, Short-chain glycoceramides promote intracellular mitoxantrone delivery from novel nanoliposomes into breast cancer cells, Pharm. Res. 32 (4) (2015) 1354–1367.
[30] R. Regev, D. Yeheskely-Hayon, H. Katzir, G.D. Eytan, Transport of anthracyclines and mitoxantrone across membranes by a flip-flop mechanism, Biochem. Pharmacol. 70 (1) (2005) 161–169.
[31] D.L. Daleke, Regulation of transbilayer plasma membrane phospholipid asymmetry, J. Lipid Res. 44 (2) (2003) 233–242.
[32] T. Pomorski, S. Hrafnsdóttir, P.F. Devaux, G. van Meer, Lipid distribution and transport across cellular membranes, Semin. Cell Dev. Biol. 12 (2) (2001) 139–148.
[33] F.M. Goñi, A. Alonso, Biophysics of sphingolipids I. Membrane properties of sphingosine, ceramides and other simple sphingolipids, Biochim. Biophys. Acta 1758 (12) (2006) 1902–1921.
[34] D. Hoekstra, O. Maier, J.M. van der Wouden, T.A. Slimane, S.C. van IJzendoorn, Membrane dynamics and cell polarity: the role of sphingolipids, 44 (5) (2003) 869–877.
[35] Sawatzki P. Megha, T. Kolter, R. Bittman, E. London, Effect of ceramide N-acyl chain and polar headgroup structure on the properties of ordered lipid domains (lipid rafts), Biochim. Biophys. Acta 1768 (9) (2007) 2205–2212.
[36] B. Maggio, M.L. Fanani, C.M. Rosetti, N. Wilke, Biophysics of sphingolipids II. Glycosphingolipids: an assortment of multiple structural information transducers at the membrane surface, Biochim. Biophys. Acta 1758 (12) (2006) 1922–1944.
[37] G. Speelmans, R.W.H.M. Staffhorst, B. de Kruijff, The anionic phospholipid-mediated membrane interaction of the anti-cancer drug doxorubicin is enhanced by phosphatidylethanolamine compared to other zwitterionic phospholipids, Biochemistry 36 (28) (1997) 8657–8662.
[38] A.B. Hendrich, K. Michalak, Lipids as a target for drugs modulating multidrug resistance of cancer cells, Curr. Drug Targets 4 (1) (2003) 23–30.
[39] G.E. Atilla-Gokcumen, E. Muro, J. Relat-Goberna, S. Sasse, A. Bedigian, M.L. Coughlin, S. Garcia-Manyes, U.S. Eggert, Dividing cells regulate their lipid composition and localization, Cell 156 (3) (2014) 428–439.
[40] C. Peetla, S. Vijayaraghavalu, V. Labhasetwar, Biophysics of cell membrane lipids in cancer drug resistance: implications for drug transport and drug delivery with nanoparticles, Adv. Drug Deliv. Rev. 65 (13–14) (2013) 1686–1698.